Molecular Weight Effect on the Absorption, Charge Carrier Mobility, and Photovoltaic Performance of an Indacenodiselenophene–Based Ladder–Type Polymer

ARTICLE *in* CHEMISTRY OF MATERIALS · JULY 2013

Impact Factor: 8.35 · DOI: 10.1021/cm401586t

CHEMISTRY OF MATERIALS

Article

pubs.acs.org/cm

Molecular Weight Effect on the Absorption, Charge Carrier Mobility, and Photovoltaic Performance of an Indacenodiselenophene-Based Ladder-Type Polymer

Jeremy J. Intemann,[†] Kai Yao,[†] Hin-Lap Yip,[†] Yun-Xiang Xu,[†] Yong-Xi Li,[†] Po-Wei Liang,[†] Fei-Zhi Ding,[‡] Xiaosong Li,[‡] and Alex K.-Y. Jen*[,†]

[†]Department of Materials Science and Engineering, and [‡]Department of Chemistry, University of Washington, Seattle, Washington 98195, United States

Supporting Information

ABSTRACT: Selenium substitution on a ladder-type indacenodithiophene-based polymer (PIDT-DFBT) is investigated in order to reduce band gap, improve charge mobilities, and enhance the photovoltaic performance of the material. The new indacenodiselenophene-based polymer (PIDSe-DFBT) possessed improved absorption over its sulfur analogue in films, as well as substantially higher charge mobilities (0.15 and 0.064 $cm^2/(V\ s)$ hole and electron mobility, respectively, compared to 0.002 and 0.008 $cm^2/(V\ s)$ for PIDT-DFBT). The enhanced material properties led to an improved power conversion efficiency of 6.8% in photovoltaic cells, a 13% improvement over PIDT-DFBT-based devices. Furthermore, we examined the effect of molecular weight on the properties of PIDSe-DFBT and found not only a strong molecular weight dependence on mobilities, but also on the absorptivity of polymer films, with each 15 000 g/mol increase in weight, leading to a 25% increase in the absorptivity of the material. The molecular weight dependence of the material's properties resulted in a significant difference in photovoltaic performance with the high-molecular-weight PIDSe-DFBT providing a higher photocurrent, fill factor, and efficiency due to its improved absorption and hole mobility. These results demonstrate the importance of achieving high molecular weight and the potential that selenium-containing ladder-type polymers have in the design of high-performance semiconducting polymers for organic photovoltaics (OPVs).

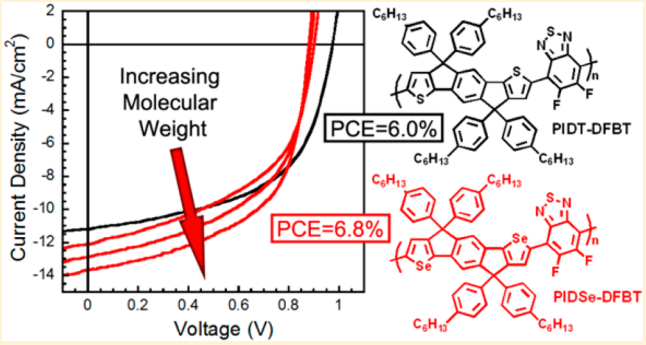

KEYWORDS: *selenium, conjugated polymers, ladder-type polymers, organic photovoltaics, organic field-effect transistors, density functional theory*

INTRODUCTION

Over the last several years, a tremendous effort has been made in the development of organic photovoltaics (OPVs) in order to achieve large-area, solution-processed, and highly efficient solar cells. The development of new semiconducting polymers with optimized frontier orbital energy levels, band gaps, charge carrier mobilities, and morphologies has allowed for power conversion efficiencies (PCEs) in excess of 8%−9% in devices.[1−4] However, to reach ever-higher efficiencies, new materials that provide higher photocurrents in OPVs through enhanced absorption of the solar photon flux and improved charge carrier mobilities must be developed.

One material design approach that has garnered attention in recent years is the incorporation of selenium in place of sulfur in the polymer backbone. Selenium substitution in moieties such as thiophene, to produce the aromatic heterocycle selenophene, is expected to have several advantages over sulfur-containing polymers. The reduced aromaticity of selenophene,[5,6] compared to thiophene, increases the ground-state quinoid resonance character of its polymers, resulting in improved planarity, increased effective conjugation length, and decreased band gap.[7,8] The decreased participation of the selenium lone pairs in aromaticity also means they are able to participate to a greater extent in intermolecular interactions, facilitating interchain charge hopping, improving charge carrier mobilities.[9] In addition, theoretical calculations have shown that the highest occupied molecular orbital (HOMO) energy level of thiophene-based polymers does not have a significant contribution from the sulfur atom, because the HOMO has a nodal plane passing through the heteroatom.[10]

Because of this, and only a marginal decrease in the electronegativity of selenium, the HOMO level is virtually unchanged. On the other hand, the lowest unoccupied molecular orbital (LUMO) is heavily influenced by the

Received: May 15, 2013
Revised: July 16, 2013
Published: July 18, 2013

heteroatom, as electron density in the LUMO is delocalized over the heteroatom. Heeney et al. demonstrated that substituting the sulfur heteroatom in regioregular poly(3-hexylthiophene) with selenium greatly stabilized the LUMO of the polymer. The decrease in the LUMO level was attributed to the lower ionization potential of selenium having a greater stabilizing effect.[11] The net result of all these contributions from selenium substitution is a slight increase in the HOMO level and a significant lowering of the LUMO. This results in a narrower band gap of the polymer for better absorption of the solar spectrum, while the relatively unchanged HOMO prevents a significant sacrifice in the open-circuit voltages (V_{oc}) in devices.

Despite these well-reasoned arguments that suggest selenium substitution should generally improve material performance, experimental findings have been highly inconsistent. Yang et al. found that replacing thiophene with selenophene as a π-bridge in a benzodithiophene-diketopyrrolopyrrole donor−acceptor copolymer, improved the hole mobility, resulting in an 11% enhancement of the PCE in devices, from 6.5% in the thiophene-based polymer, to 7.2% in the selenophene analogue.[12] Yu et al. also reported similar results from selenium incorporation into both the donor and acceptor moieties in a benzodithiophene-thieno[3,4-b]thiophene copolymer, with enhanced mobilities from space-charge limited-current measurements and improved device efficiencies.[13] Conversely, Chen et al. reported the use of thiophene and selenophene bridged donor−acceptor polymers using benzodithiophene and carbazole-based donors copolymerized with a dialkoxy benzothiadiazole acceptor. They found that selenium substitution in the carbazole-containing polymers improved mobility and device efficiencies, while selenium substitution in the benzodithiophene-based polymers showed reduced mobilities and device performance,[14] and there are many similar reports with polymers showing reduced mobility and performance when sulfur is substituted with selenium.[15−17] The seemingly contradictory nature of these findings suggests that further investigation into the effects of selenium substitution in semiconducting polymers is needed.

One potential problem with selenium-containing polymers arises from an increase in van der Waals forces, which is due to the greater polarizability of selenium. This decreases the solubility of its polymers, relative to thiophene. As a result, it can often be difficult to obtain these polymers with high molecular weights,[16,18] which has been shown to be crucial for achieving high mobilities and efficiencies in devices.[19−25] Because of this, a detailed study of the significance of molecular weight and its impact on the properties and performance of selenium-containing polymers is needed in order to understand if comparisons between lower-molecular-weight selenium-containing polymers and higher-molecular-weight sulfur-based polymers are reasonable.

Aside from heteroatom substitution, another design strategy that has proven useful in the development of high performance polymers is the fusing of aromatic rings into extended ladder-like structures. These types of moieties are interesting because the highly coplanar structure gives the polymers containing them excellent optical and electronic properties, such as increased absorption coefficients, decreased reorganizational energies, and improved charge carrier mobilities.[26−32] Among ladder-type donors, indacenodithiophene (IDT) has been one of the most widely studied, having been made with a large variety of different acceptors,[33−41] producing power conversion efficiencies as high as 7.5% in OPVs.[42,43] Previously, we reported an IDT-difluorobenzothiadiazole donor−acceptor copolymer (PIDT-DFBT) with good performance in OPVs.[41] The weak donating strength of IDT, combined with the HOMO stabilizing effects of the fluorine atoms,[44] resulted in a low lying HOMO and high open-circuit voltages in devices, providing a high PCE of 5.97%.[26,45] One of the main constraints of this polymer is its wide optical gap of 1.79 eV, which limited its ability to absorb light in a wide region of the solar spectrum. In order to reduce the optical gap of IDT-DFBT, and further improve the charge carrier mobilities of the material, we explored substituting the sulfur atoms of the IDT moiety with selenium (Scheme 1) to produce the first selenium-substituted ladder-type donor−acceptor polymer, PIDSe-DFBT. In addition, PIDSe-DFBT was prepared in three different molecular weights to evaluate the effect of polymer length on material and device properties.

Scheme 1. Structures of PIDT-DFBT and PIDSe-DFBT

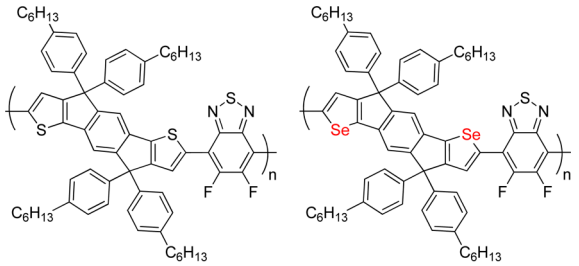

RESULTS AND DISCUSSION

Synthesis and Characterization. The synthetic route used to make the PIDSe-DFBT polymer is shown in Scheme 2.

Scheme 2. Synthesis of PIDSe-DFBT

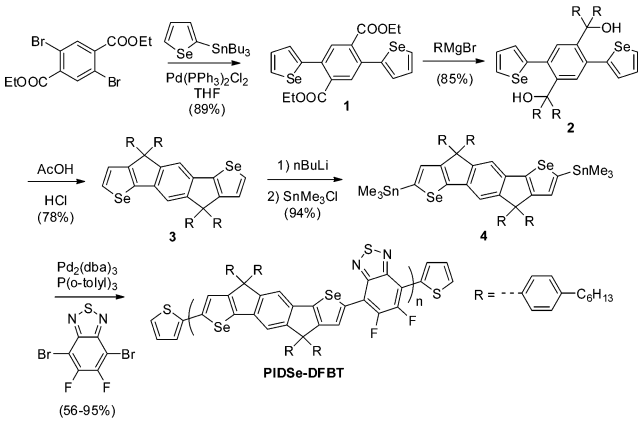

Compound **1** was prepared by Stille cross-coupling between 2,5-dibromoterephthalic ethyl ester and 2-tributyltinselenophene with a palladium(II) catalyst. The side chains were then attached by the addition of 4-hexylphenylmagnesium bromide to make compound **2**. Compound **3** was then made via acid-catalyzed Friedel−Crafts cyclization, which was then converted to compound **4** using *n*-butyllithium and trimethyltin chloride. The polymerization of IDSe-DFBT was carried out via a Stille polymerization with compound **4** and 4,7-dibromo-5,6-difluoro-[2,1,3]benzothiadiazole using catalytic $Pd_2(dba)_3$ and

dx.doi.org/10.1021/cm401586t | Chem. Mater. 2013, 25, 3188−3195

Table 1. Physical, Optical, and Electrochemical Properties of PIDT-DFBT and PIDSe-DFBT

polymer	M_n (kg/mol)	PDI	λ_{max}^{soln} (nm)[a]	λ_{max}^{film} (nm)	E_g^{opt} (eV)[b]	E_{HOMO} (eV)[c]	E_{LUMO} (eV)[c]	E_g^{ec} (eV)
PIDT-DFBT	61.4	3.04	634	647	1.79	−5.35	−3.40	1.95
PIDSe-DFBT$_L$	30.1	2.21	669	671	1.68	−5.34	−3.48	1.86
PIDSe-DFBT$_M$	46.3	2.37	671	670	1.68	−5.34	−3.47	1.87
PIDSe-DFBT$_H$	61.8	2.07	672	673	1.68	−5.33	−3.48	1.85

[a]Taken in dilute chlorobenzene solutions. [b]Calculated from the absorption onset of the film spectra. [c]Calculated from the oxidation and reduction onsets from CV measurements referenced to ferrocene, using the equation $E_{HOMO/LUMO} = -4.8 - E_{redox}$.

a P(*o*-tolyl)$_3$ ligand. In order to obtain PID-Se-DFBT with different molecular weights, reaction conditions of the polymerization were carefully modified.

To obtain the low-molecular-weight polymer (PIDSe-DFBT$_L$), the polymerization was carried out in chlorobenzene using a small stoichiometric imbalance between the donor and acceptor monomers. The midmolecular weight polymer (PIDSe-DFBT$_M$), on the other hand, was made using a properly balanced ratio of monomers, but polymerized in toluene. The poor solubility of PIDSe-DFBT in toluene caused the polymer to precipitate out of the reaction before achieving a higher molecular weight. The high-molecular-weight polymer (PIDSe-DFBT$_H$) was obtained under the same conditions as PIDSe-DFBT$_M$, except the polymerization was carried out in chlorobenzene, which better solubilized the polymer, preventing it from precipitating out during the polymerization. The molecular weights of the PIDSe-DFBT polymers are summarized in Table 1.

PIDSe-DFBT$_L$ and PIDSe-DFBT$_M$ possessed good solubility in common organic solvents such as chloroform, toluene, chlorobenzene, and dichlorobenzene, while PIDSe-DFBT$_H$ was only soluble in chlorobenzene and dichlorobenzene, although its solubility in those solvents was excellent. The molecular weights of the PIDSe-DFBT polymers increases by ∼15 kg/mol in each sample to give a molecular weight range of 30.1−61.8 kg/mol, and the high-molecular-weight polymer is nearly identical to the molecular weight of PIDT-DFBT, allowing for a good comparison of the effects of heteroatom substitution.

Thermal analysis using differential scanning calorimetry (DSC) yielded no thermal transition for any of the PIDSe-DFBT samples (see Figure S1 in the Supporting Information (SI)), indicating that these polymers do not possess a glass-transition temperature. This is a known trait of IDT-based polymers that possess alkyl phenyl side chains, because the phenyl groups extend out of the plane of the polymer backbone, disrupting π-stacking interactions and preventing crystallization of the polymer.[34,46]

Photophysical and Electrochemical Properties. The optical properties of the polymers were investigated using UV−vis spectroscopy. The UV absorption spectra of PIDSe-DFBT was almost identical for the three different molecular weights in both solution and film (Figure 1), suggesting all three polymers possess backbones longer than the effective conjugation length of the polymer. The PIDSe-DFBT polymers displayed a red-shift relative to PIDT-DFBT of ∼27 nm in thin films and had smaller optical gaps, with PIDSe-DFBT possessing an optical gap of 1.68 eV, compared to 1.79 eV for PIDT-DFBT. There is no meaningful red-shift between solution and film for any of the polymers, likely due to the out-of-plane alkylphenyl side chains preventing efficient packing of the polymer backbones, since polymer concentration and varied temperature has no effect on the absorption spectra of the solutions (see Figure S2 in the SI).

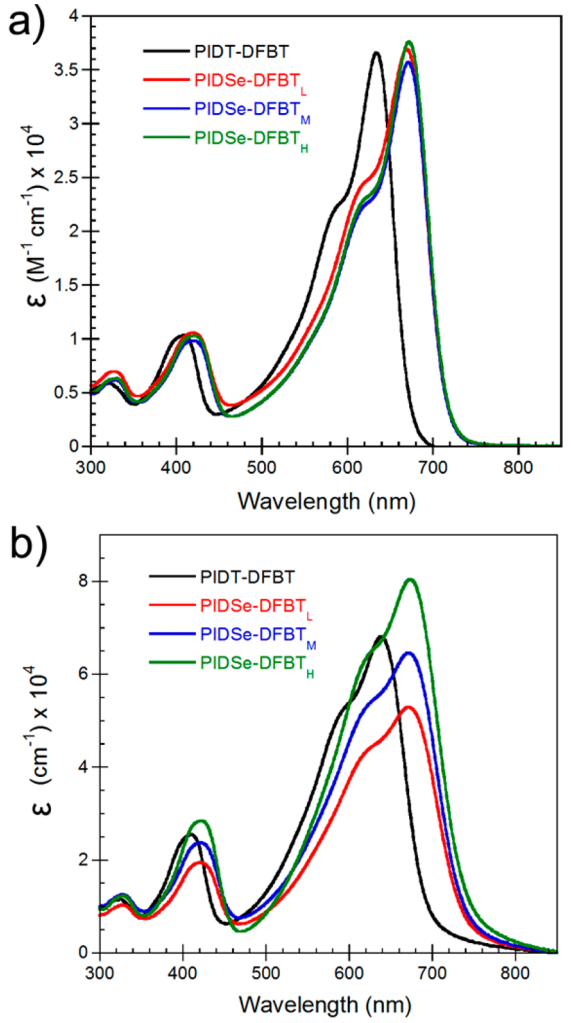

Figure 1. UV−vis spectra and extinction coefficients of polymers in (a) dilute chlorobenzene solutions and (b) thin films.

The extinction coefficients of the polymers in solution show no effect from either chalcogen substitution of molecular weight; however, these factors show a significant effect in thin films. Selenium substitution caused an increase in the film extinction coefficient when comparing similar molecular weight polymers, while increasing the molecular weight leads to an increased absorptivity. The reason for this difference between solution and film properties may be the result of differences in film densities. For example, replacing sulfur with selenium in conjugated polymers has been shown to decrease lamellar packing distances and increase packing density in films.[9] Increasing the molecular weight of the polymer may also lead to differences in packing and film density; however, because of the amorphous packing of these polymers, their morphology cannot be investigated via X-ray diffraction (XRD) experiments.

dx.doi.org/10.1021/cm401586t | *Chem. Mater.* 2013, 25, 3188−3195

The frontier orbital energy levels of the polymers were measured using cyclic voltammetry (CV) on polymer films. The CV traces for the polymers referenced to ferrocene can be seen in Figure S3 in the SI. The HOMO and LUMO energy levels were estimated from the onsets of the oxidation and reduction waves, and the results are summarized in Table 1. As expected, selenium substitution leads to only a small destabilization of the HOMO level in PIDSe-DFBT, compared to PIDT-DFBT; however, the LUMO level has been reduced by ~0.08 eV, because of the stabilizing effect of the selenium in the backbone. The HOMO/LUMO energies for the different molecular weight PIDSe-DFBT are all fairly similar, in good agreement with the absorption spectra, and demonstrating that increasing the molecular weight has a negligible impact of the electronic properties of the polymers. The electrochemical gaps are all slightly higher than the optical gaps; however, they clearly show the same general trend that selenium substitution leads to a decrease of ~0.1 eV in the optical and electrochemical gaps of the polymers. The decreased electrochemical gap and increased absorption of the PIDSe-DFBT film should result in better harvesting of solar photon flux, while the still low-lying HOMO level should lead to only a small sacrifice in open-circuit voltage in devices.

Quantum chemical calculations were performed on analogous trimer models of PIDT-DFBT and PIDSe-DFBT, in order to gain a better insight into the effect of heteroatom substitution in these materials. The spatial geometries of the trimers were optimized and the HOMO and LUMO wave functions were examined, the results of which are summarized in Table 2. The predicted HOMO and LUMO values of the

Table 2. Density Functional Theory (DFT)-Calculated Orbital Energy Levels

trimer	HOMO (eV)	LUMO (eV)	E_g (eV)
PIDT-DFBT	−4.67	−2.79	1.88
PIDSe-DFBT	−4.64	−2.84	1.80

trimers follow the same trends as the experimental data of the polymers. The HOMO of the PIDSe-DFBT-based trimer is slightly elevated compared to the sulfur analogue, with a larger stabilization of the LUMO in the selenium substituted trimer. Calculations predict that selenium substitution will decrease the HOMO−LUMO gap by 0.08 eV, similar to the observed decrease of 0.11 eV in the optical gap and the 0.09 eV decrease in the electrochemical gap.

The predicted oscillator strengths of the modeled trimers (Figure 2) are also in good agreement with the extinction coefficients of the polymers in solution. DFT calculations do not predict a significant change in the oscillator strength of the trimers, further suggesting the differences in absorptivity between solution and film are the result of morphology and not due to the material's electronic properties.

Charge Mobilities. Organic field-effect transistors (OFETs) with a bottom-gate and top-contact configuration were fabricated to examine the effect of heteroatom substitution and molecular weight on the charge mobilities of PIDSe-DFBT. The results of the transfer curves of devices are summarized in Table 3. As expected, the molecular weight of PIDSe-DFBT has a significant impact on both hole and electron mobilities. The low-molecular-weight PIDSe-$DFBT_L$ has similar hole and electron mobilities as PIDT-DFBT. When the molecular weight is increased by ~15 kg/mol, both the hole and electron

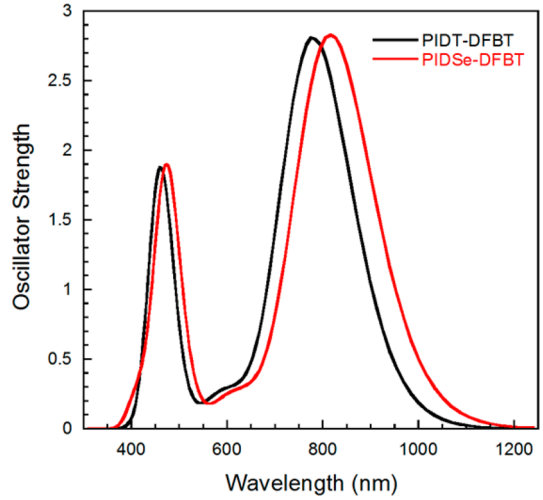

Figure 2. Density functional theory (DFT)-calculated (B3LYP/6-31G*) oscillator strength of modeled trimers.

Table 3. Organic Field-Effect Transistor (OFET) Device Characteristics[a]

polymer	$\mu_{sat,h}$ ($cm^2/(V\ s)$)	$I_{on/off,\ h}$	$\mu_{sat,e}$ ($cm^2/(V\ s)$)	$I_{on/off,\ e}$
PIDT-DFBT[b]	0.002	2×10^3	0.008	1×10^3
PIDSe-$DFBT_L$	0.002 ± 0.001	4.4×10^3	0.008 ± 0.002	2.7×10^4
PIDSe-$DFBT_M$	0.006 ± 0.002	9.3×10^3	0.030 ± 0.010	2.0×10^3
PIDSe-$DFBT_H$	0.15 ± 0.04	6.0×10^2	0.064 ± 0.015	1.4×10^2

[a]Average values from eight devices. [b]Values from the literature.[26]

mobilities increase by a factor ~3−4 in PIDSe-$DFBT_M$. Further increasing the molecular weight by ~15 kg/mol leads to an enhancement in the hole mobility by nearly 2 orders of magnitude, which is accompanied by only a small increase in the electron mobility. Improved mobilities with higher-molecular-weight polymers has been reported previously, and has been attributed to improved π-stacking, film-forming properties, and increased interchain overlap, leading to increased polaron delocalization.[19,21] In previous investigations into the effect molecular weight has on mobility, only two different molecular weights have been compared, so the exact relationship between mobility and polymer weight is not well understood and may not be linear. The moderate improvement in hole mobility between the low-molecular-weight and mid-molecular-weight polymers, followed by the large improvement seen in the high-molecular-weight polymer, is surprising and warrants further study. Compared to PIDT-DFBT, PIDSe-$DFBT_H$ shows a two-order-of-magnitude increase in the hole mobility and an order-of-magnitude increase in the electron mobility. The improvement in mobility likely originates from Se−Se interactions due to the larger, more-polarizable Se atom.[18,47−49]

Photovoltaic Properties. The effect of selenium substitution on the photovoltaic properties of the materials was investigated using a device configuration of ITO/PEDOT:PSS/polymer:$PC_{71}BM$/Bis-C_{60}/Ag. We previously reported PCEs as high as 5.97% in PIDT-DFBT-based devices using an identical device configuration with a 1:3 polymer:fullerene weight-to-weight ratio (w/w);[26] however, we found that increasing the w/

dx.doi.org/10.1021/cm401586t | Chem. Mater. 2013, 25, 3188−3195

w ratio to 1:4 resulted in slightly improved efficiencies. A 1:4 ratio was also found to be the optimum blend for the PIDSe-DFBT polymers, and the resulting $J-V$ curves are shown in Figure 3a.

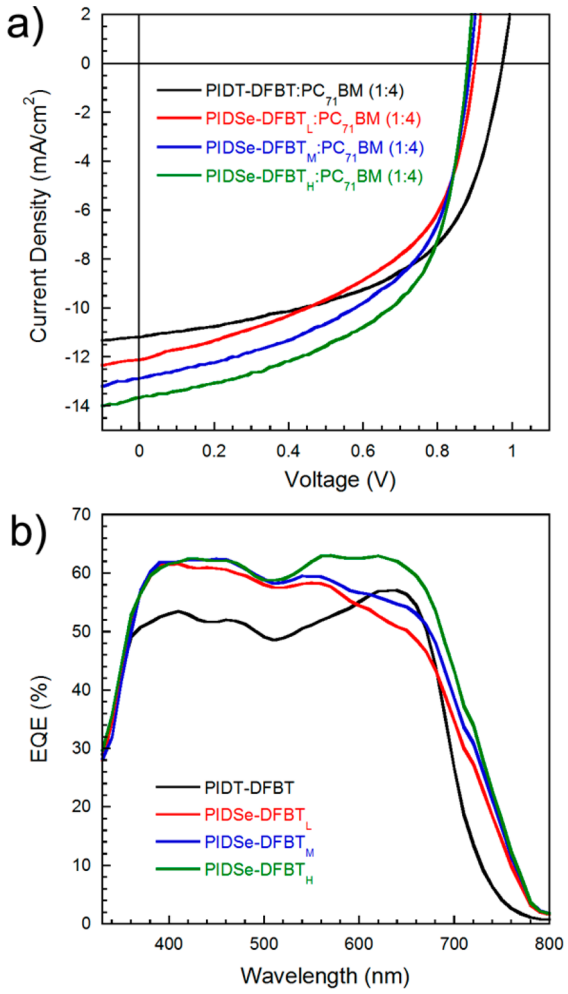

Figure 3. Characteristic (a) current density–voltage ($J-V$) curves and (b) external quantum efficiency (EQE) curves of BHJ polymer solar cells under AM1.5G, 100 mW/cm^2 illumination.

Among the PIDSe-DFBT polymers, molecular weight clearly played an important role in the device performance. The short-circuit current density (J_{sc}) steadily increases as the molecular weight increases. The increased J_{sc} is the result of the improved absorption and hole mobility with increased molecular weight. The fill factor (FF) also steadily increases with higher molecular weight, because of the improved hole mobility, facilitating charge collection and limiting recombination. The external quantum efficiency (EQE) of the devices (Figure 3b) is in good agreement with these observations as the EQE increases with molecular weight in the 550–700 nm range, where the polymer absorption is primarily responsible for exciton generation. The increasing EQE mirrors the increasing absorptivity seen in the PIDSe-DFBT polymer films. The improved efficiencies with increasing molecular weight appears to be primarily related to the increased optical absorption and hole mobilities, as atomic force microscopy (AFM) height images (see Figure S6 in the SI) show no discernible change in the film morphology with increasing molecular weight.

Selenium substitution also has a dramatic impact on device performance, as an increase of 2.5 mA/cm^2 in the J_{SC} is observed between PIDT-DFBT and PIDSe-DFBT$_H$. The increase in J_{SC} is due to the optical gap, improved solid-state absorptivity, and higher hole mobility of the PIDSe-DFBT$_H$ polymer, compared to the sulfur analogue. The fill factor (FF) is also slightly improved in PIDSe-DFBT$_H$, because of the increased mobility, which leads to a decrease in charge recombination. Selenium substitution, as expected, results in a sacrifice of the V_{oc} (~0.08 V), due to the slightly higher-lying HOMO in PIDSe-DFBT, however, the improved J_{SC} and FF values make up for this loss to give the PIDSe-DFBT$_H$ device a higher PCE of 6.79% than the 6.02% of the PIDT-DFBT device. AFM images of both the PIDT-DFBT and PIDSe-DFBT$_H$ heterojunction show good dispersion of the polymers in PCBM with similar root-mean-square (RMS) roughness values of 0.86 and 0.56 nm, respectively, indicating comparable film morphologies.

Table 4. Photovoltaic Properties of Polymers

device[a]	J_{SC} (mA/cm^2)	V_{OC} (V)	fill factor, FF (%)	η (%)[b]
PIDT-DFBT	11.2	0.97	55.4	6.02 (5.87 ± 0.13)
PIDSe-DFBT$_L$	12.1	0.90	50.3	5.48 (5.17 ± 0.24)
PIDSe-DFBT$_M$	12.9	0.89	53.2	6.11 (5.92 ± 0.15)
PIDSe-DFBT$_H$	13.7	0.89	56.3	6.79 (6.61 ± 0.12)

[a]Devices based on a ITO/PEDOT:PSS/polymer:PC$_{71}$BM (1:4)/Bis-C$_{60}$/Ag structure, using a 1:4 polymer:fullerene (w/w) ratio. [b]Champion values with average values and standard deviation in parentheses, averaged from eight devices.

CONCLUSION

In summary, we have reported the new selenium-substituted ladder-type PIDSe-DFBT with three different molecular weights. A strong correlation between the material's molecular weight and the film absorptivity, charge carrier mobilities, and photovoltaic performance was found, with the highest-molecular-weight polymer providing the best performance in those categories. The effect of selenium substitution in PIDT-DFBT lead to a reduced band gap from a lower-lying LUMO, enhanced hole and electron mobilities, increased film absorptivity, and improved photovoltaic performance. These results demonstrate the importance of achieving high molecular weight and the potential that selenium-containing ladder-type polymers have in the design of high-performance semiconducting polymers for OPVs.

EXPERIMENTAL DETAILS

Materials and Characterization. All materials were purchased from Aldrich, unless otherwise stated. Diethyl 2,5-dibromotereph-thalate[50] and 4,7-dibromo-5,6-difluoro-[2,1,3] benzothiadiazole[41] were prepared according to literature procedures. Ultraviolet–visible light (UV–vis) spectra were measured using a Perkin–Elmer Lambda-9 spectrophotometer. The thickness of the polymer films was measured by scratching the center of the polymer films and measuring its depth using tapping-mode atomic force microscopy (AFM). The depth was measured at several positions, and the heights were averaged. The films were all highly uniform with a 2% deviation in the height measurements. The absorption of the films was then normalized to a thickness of 1 cm to determine the extinction coefficient. The ^{1}H and ^{13}C NMR spectra were collected on a Bruker AV 300 and AV500 spectrometers operating at 300 and 125 MHz in deuterated

dx.doi.org/10.1021/cm401586t | Chem. Mater. 2013, 25, 3188–3195

chloroform solution referenced to TMS. Gel permeation chromatography (GPC) measurements were performed on a Waters GPC system, using a Model 1515 isocratic pump and a refractive index detector with an *o*-dichlorobenzene mobile phase at 130 °C. Thermal transitions were measured on a TA Instruments Q20-1066 differential scanning calorimeter with a heating rate of 10 °C min^{-1}. Cyclic voltammetry of polymer films was conducted in a 0.1 M tetrabutylammonium hexafluorophosphate solution in acetonitrile, using a scan rate of 100 mV s^{-1}. ITO, Ag/AgCl, and Pt mesh were used as the working electrode, reference electrode, and counter electrode, respectively. High-resolution mass spectroscopy (HRMS) measurements were performed on a Bruker Apex-Qe FT/ICR from the Medicinal Chemistry Department at University of Washington.

Synthetic Methods. *2,5-Di(selenophen-2-yl)terephthalic Ethyl Ester (1).* A solution of selenophene (2.16 g, 16.5 mmol) and tetrahydrofuran (THF) (14 mL) were cooled to −30 °C under nitrogen and a 2.5 M *n*-butyllithium solution in hexane (6.6 mL, 16.5 mmol) was added dropwise. The mixture was stirred for 4 h and then tributyltin chloride (5.3 mL, 19.8 mmol) was added. The mixture was stirred for another hour and then saturated aqueous $NaHCO_3$ was added to quench the reaction. The organic phase was separated, washed with more $NaHCO_3$, followed by washing with brine. The solvent was then removed under reduced pressure. The tributyltin selenophene was then dissolved in THF (100 mL) and 2,5-dibromoterephthalate diethyl ester (2.85 g, 7.5 mmol) was added. The mixture was deoxygenated by bubbling nitrogen gas through it for 30 min and then $Pd(PPh_3)_4Cl_2$ (263 mg, 5 mol %) was added. The mixture was then refluxed for 2 days and then cooled to room temperature. The solvent was evaporated and the crude product was purified on a silica gel column using 6:1 hexanes:ethylacetate as the eluent. Evaporation of the solvent yielded the product as a white solid (3.21 g, 89% yield). ^{1}H NMR (500 MHz, CDCl3, δ): 8.08 (dd, J = 5.6 Hz, 1.1 Hz, 2H), 7.78 (s, 2H), 7.30 (dd, J = 5.6 Hz, 3.8 Hz, 2H), 7.22 (dd, J = 3.7 Hz, 1.1 Hz, 2H), 4.21 (q, J = 7.2 Hz, 4 H), 1.15 (t, J = 7.1 Hz, 6H); ^{13}C NMR (500 MHz, $CDCl_3$, δ): 167.8, 135.5, 134.8, 133.7, 132.4, 131.8, 129.7, 129.3, 61.7, 13.8; HRMS-ESI $(M+Na)^+$: Calcd 504.9428; Found 504.9464.

(2,5)-Di(selenophen-2-yl)-1,4-phenylene)bis(di(4-hexylphenyl)-methanol (2). 1-Bromo-4-hexylbenzene (7.92 g, 32 mmol) was dissolved in THF (38 mL) and placed under a nitrogen atmosphere. The solution was cooled to −78 °C and stirred while 2.5 M *n*-butyllithium in hexane (12.7 mL, 32 mmol) was added dropwise. The mixture was stirred for 1 h and then a solution of **1** (3.15 g, 6.6 mmol) in THF (25 mL) was added dropwise. The reaction was warmed to room temperature and stirred overnight. It was then poured into water and extracted with dichloromethane (3 × 75 mL). The organic extracts were combined and dried over anhydrous Na_2SO_4. After removal of the solvent, the crude product was recrystallized from a small amount of ethyl acetate to yield a white solid (5.83 g, 85% yield). ^{1}H NMR (500 MHz, $CDCl_3$, δ): 7.85 (dd, J = 5.6 Hz, 1.0 Hz, 2H), 7.09 (br s, 16H), 6.93 (dd, J = 5.7 Hz, 3.8 Hz, 2H), 6.70 (s, 2H), 6.36 (dd, J = 3.7 Hz, 1 Hz, 2H), 3.62 (s, 2H), 2.60 (t, J = 7.5 Hz, 8H), 1.60 (m, J = 7.2 Hz, 8H), 1.29 (br m, 24H), 0.88 (t, J = 6.7 Hz, 12H); ^{13}C NMR (500 MHz, $CDCl_3$, δ): 184.8, 144.8, 144.5, 142.0, 136.2, 133.7, 130.4, 129.0, 128.0, 127.9, 82.8, 35.5, 31.8, 31.4, 28.8, 22.7, 14.2; HRMS-ESI $(M+Na)^+$: Calcd 1061.4224; Found 1061.4561.

4,4,9,9-Tetrakis(4-hexylphenyl)indaceno[1,2-b:5,6-b′]-diselenophene (3). To a refluxing mixture of **2** (2.29 g, 2.2 mmol) in acetic acid (44 mL) was added concentrated HCl (4.4 mL) in a dropwise fashion. The mixture was refluxed for 3 h and then poured into water. The precipitate was collected and washed repeatedly with methanol. The crude product was then purified on a silica gel column using 10:1 hexane:dichloromethane as the eluent. Evaporation of the solvent yielded an off-white solid (1.71 g, 78% yield). ^{1}H NMR (500 MHz, $CDCl_3$, δ): 7.87 (d, J = 5.3 Hz, 2H), 7.39 (s, 2H), 7.20 (d, J = 5.4 Hz, 2H), 7.14 (d, J = 8.2, 8H), 7.04 (d, J = 8.2, 8H), 2.55 (t, J = 7.7 Hz, 8H), 1.58 (br m, 8H), 1.29 (br m, 24H), 0.87 (t, J = 6.9 Hz, 12H); ^{13}C NMR (500 MHz, $CDCl_3$, δ): 157.5, 152.8, 144.2, 141.9, 141.3, 137.5, 131.8, 128.3, 127.9, 117.6, 63.9, 35.6, 31.7, 31.3, 29.2, 22.6, 14.1; HRMS-ESI ($M^{\bullet+}$): Calcd 1002.4115; Found 1002.4067.

4,4,9,9-Tetrakis(4-hexylphenyl)-2,7-bis(trimethylstannyl)-indaceno [1,2-b:5,6-b′]Diselenophene (4). Compound **3** (292 mg, 0.28 mmol) was dissolved in THF (5.7 mL) and stirred at −78 °C, under a nitrogen atmosphere, while a 2.5 M solution of *n*-butyllithium in hexane (0.34 mL, 0.85 mmol) was added dropwise. The mixture was stirred for 30 min, then warmed to 0 °C and stirred another 30 min before cooling the reaction back down to −78 °C. A 1.0 M solution of trimethyltin chloride in THF (1.13 mL) was then added dropwise. The reaction was then warmed to room temperature and stirred overnight. The mixture was poured into water and extracted with dichloromethane (3 × 30 mL). The organic phases were combined, washed with brine, and dried over Na_2SO_4. Evaporation of the solvent yielded an oil, to which methanol was added. The precipitated product was collected by filtration, washing with methanol, yielding the product as an off-white solid (351 mg, 94% yield). ^{1}H NMR (500 MHz, $CDCl_3$, δ): 7.34 (s, 2H), 7.28 (s, 2H), 7.14 (d, J = 8.2 Hz, 8H), 7.04 (d, J = 8.1 Hz, 8H), 2.55 (t, J = 7.7 Hz, 8H), 1.58 (br m, 8H), 1.29 (br m, 24H), 0.87 (t, J = 6.8, 12H), 0.32 (s, 18H). HRMS-ESI ($M^{\bullet+}$): Calcd 1330.3411; Found 1330.3496.

Polymerization of PIDSe-DFBT$_L$. Compound **4** (133 mg, 0.100 mmol) and 4,7-dibromo-5,6-difluoro-[2,1,3]benzothiadiazole (34.6 mg, 0.105 mmol) were dissolved in chlorobenzene (3.5 mL) and deoxygenated by bubbling nitrogen through the solution for 30 min. $Pd_2(dba)_3$ (1.8 mg, 2 mol %) and tri-*o*-tolylphosphine (2.5 mg, 8 mol %) were then added and the mixture was heated to 125 °C for 24 h. A drop of 2-bromothiophene was then added and the reaction was stirred at 125 °C for an additional 3 h. Two drops of 2-tributylstannylthiophene was then added and the reaction was stirred at 125 °C overnight. The polymer was then precipitated into methanol and then washed sequentially with methanol, acetone, and hexane in a Soxhlet extractor. The polymer was then extracted with chloroform and then passed through a plug of silica gel (~2 cm in diameter × 6 cm in length). The dissolved polymer was concentrated and then precipitated into methanol to yield a blue solid (104 mg, 89% yield). ^{1}H NMR (300 MHz, $CDCl_3$, δ): 8.37 (br s, 2H), 7.52 (s, 2H), 7.25 (d, J = 7.8 Hz, 8H), 7.10 (d, J = 8.1 Hz, 8H), 2.57 (t, J = 7.4 Hz, 8H), 1.58 (br m, 8H), 1.30 (br m, 24H), 0.86 (t, J = 5.9 Hz, 12H); Anal. Calcd for $C_{70}H_{72}F_2N_2SSe_2$: C, 71.90; H, 6.21; N, 2.40. Found: C, 70.82; H, 5.90; N, 2.16; GPC (*o*-dichlorobenzene): M_n = 30 100 g/mol, M_w = 66 500 g/mol, PDI = 2.21.

Polymerization of PIDSe-DFBT$_M$. Compound **4** (279 mg, 0.21 mmol) and 4,7-dibromo-5,6-difluoro-[2,1,3] benzothiadiazole (66 mg, 0.2 mmol) were dissolved in toluene (7 mL) and deoxygenated by bubbling nitrogen through the solution for 30 min. $Pd_2(dba)_3$ (3.7 mg, 2 mol %) and tri-*o*-tolylphosphine (4.9 mg, 8 mol %) were then added and the mixture was heated to reflux for 24 h. A drop of 2-bromothiophene was then added and the reaction was refluxed for an additional 3 h. Two drops of 2-tributylstannylthiophene was then added and the reaction was refluxed overnight. The polymer was then precipitated into methanol and then washed sequentially with methanol, acetone, and hexane in a Soxhlet extractor. The polymer was then extracted with chloroform and passed through a plug of silica gel (~2 cm in diameter × 6 cm in length). The dissolved polymer was concentrated and then precipitated into methanol to yield a blue solid (122.2 mg, 52% yield). ^{1}H NMR (300 MHz, $CDCl_3$, δ): 8.37 (br s, 2H), 7.51 (s, 2H), 7.25 (d, J = 8.6 Hz, 8H), 7.10 (d, J = 8.0 Hz, 8H), 2.57 (t, J = 7.1 Hz, 8H), 1.55 (br m, 8H), 1.30 (br m, 24H), 0.86 (t, J = 6.8 Hz, 12H); Anal. Calcd for $C_{70}H_{72}F_2N_2SSe_2$: C, 71.90; H, 6.21; N, 2.40. Found: C, 71.16; H, 5.91; N, 2.16; GPC (*o*-dichlorobenzene): M_n = 46 300 g/mol, M_w = 109 700 g/mol, PDI = 2.37.

Polymerization of PIDSe-DFBT$_H$. Compound **4** (140.2 mg, 0.106 mmol) and 4,7-dibromo-5,6-difluoro-[2,1,3]benzothiadiazole (33.2 mg, 0.101 mmol) were dissolved in chlorobenzene (3.5 mL) and deoxygenated by bubbling nitrogen through the solution for 30 min. $Pd_2(dba)_3$ (1.8 mg, 2 mol %) and tri-*o*-tolylphosphine (2.5 mg, 8 mol %) were then added and the mixture was heated to 125 °C for 24 h. A drop of 2-bromothiophene was then added and the reaction was stirred at 125 °C for an additional 3 h. Two drops of 2-tributylstannylthiophene were added and the reaction was stirred at 125 °C overnight. The polymer was precipitated into methanol and

dx.doi.org/10.1021/cm401586t | *Chem. Mater.* 2013, 25, 3188−3195

then washed sequentially with methanol, acetone, hexane, and chloroform in a Soxhlet extractor. The polymer was then extracted with chlorobenzene and passed through a plug of silica gel (~2 cm in diameter × 6 cm in length). The dissolved polymer was concentrated and precipitated into methanol to yield a blue solid (112.2 mg, 95% yield). Becuase of the insolubility of PIDSe-DFBT$_H$ in chloroform, no NMR data are available for this polymer. Anal. Calcd for $C_{70}H_{72}F_2N_2SSe_2$: C, 71.90; H, 6.21; N, 2.40. Found: C, 71.48; H, 5.91; N, 2.11. GPC (*o*-dichlorobenzene): M_n = 61 800 g/mol, M_w = 127 900 g/mol, PDI = 2.07.

Computational Methods. To facilitate an in-depth understanding of the electronic structure of the polymers, we have performed density functional theory (DFT) calculations for the model trimers. The hybrid B3LYP [1-3] functional and a 6-31G(d) basis set were used to obtain the optimized structures at the singlet ground state. For the sake of computational efficiency, the hexyl chains appended to the conjugated backbone were replaced with methyl groups. The first excited singlet states as well as other low-lying excited states for the two trimers were calculated at the optimized ground state geometries within the linear-response time-dependent DFT (LR-TDDFT) framework. All calculations were performed using the GAUSSIAN 09 program package.

Organic Field-Effect Transistor Fabrication. Field-effect transistors were fabricated through the top-contact and bottom-gate geometry. Heavily doped *p*-type silicon ⟨100⟩ substrates with a 300-nm thermal oxide layer were purchased from Montco Silicon Technologies INC. After cleaning the substrate by sequential ultrasonication in acetone and isopropyl alcohol for 15 min followed by air plasma treatment, the oxide layer was passivated with a thin divinyltetramethyldisiloxane-bis(benzocyclobutene) (BCB) buffer layer. Polymer thin films were spin-coated from a 0.5 wt % *o*-dichlorobenzene solution. Interdigitated source and drain electrodes (W = 1000 mm, L = 20/30 mm) were defined by evaporating Au (40 nm) through a shadow mask from the resistively heated Mo boat at 10^{-7} Torr. OFET characterization was carried out in a N_2-filled glovebox using an Agilent Model 4155B semiconductor parameter S6 analyzer. The field-effect mobility was calculated in the saturation regime from the linear fit of $(I_{ds})^{1/2}$ vs V_{gs}. The threshold voltage (V_t) was estimated as the *x*-intercept of the linear section of the plot of $(I_{ds})^{1/2}$ vs V_{gs}. The subthreshold swing was calculated by taking the inverse of the slope of I_{ds} vs V_{gs} in the region of exponential current increase.

Photovoltaic Device Fabrication. Photovoltaic cells were fabricated using indium tin oxide (ITO)-coated glass substrates (15 $\Omega\,\square^{-1}$), which were cleaned with detergent, deionized water, acetone, and isopropyl alcohol. A thin layer (~35 nm) of PEDOT:PSS (Baytron P VP AI 4083, filtered at 0.45 μm) was first spin-coated on the precleaned ITO-coated glass substrates at 5000 rpm and baked at 140 °C for 10 min in air. The substrates were then transferred into a N_2-filled glovebox and the polymer:PC71 BM active layer (~90 nm) was spin-coated on the PEDOT:PSS layer from a homogeneous solution. The solution was prepared by dissolving the polymer and fullerene at different weight ratios in *o*-dichlorobenzene overnight and filtered through a polytetrafluoroethylene (PTFE) filter (0.45 μm). A bis-C_{60} fullerene surfactant layer[51,52] was further spun onto the active layer and then thermally annealed at 110 °C for 5 min. Finally, Ag (100 nm) was thermally evaporated under high vacuum (<2 × 10^{-6} Torr) to serve as the cathode. J–V curves were recorded using a Keithley 2400 source measure unit. The device photocurrent was measured under illumination from a 450 W Thermal Oriel solar simulator (AM 1.5G). The illumination intensity of the light source was accurately calibrated employing a standard Si photodiode detector equipped with a KG-5 filter, which can be traced back to the standard cell of the National Renewable Energy Laboratory (NREL). The calibration method, based on the IEC-69094-1 spectrum, followed procedures described previously. The EQE spectra performed here were obtained by the IPCE measurement using the combination of a xenon lamp (Oriel, 450 W) as the light source, a monochromator, chopper with a frequency of 100 Hz, a lock-in amplifier (SR830, Stanford Research Corp.), and a Si-based diode (Model J115711-1-Si detector) for calibration.

■ ASSOCIATED CONTENT

Ⓢ Supporting Information

Differential scanning calorimetry data, cyclic voltammetry traces, DFT-calculated optimized structures, OFET transfer curves, and AFM height images. This material is available free of charge via the Internet at http://pubs.acs.org.

■ AUTHOR INFORMATION

Corresponding Author

*E-mail: ajen@u.washington.edu.

Notes

The authors declare no competing financial interest.

■ ACKNOWLEDGMENTS

The authors thank the support from the Air Force Office of Scientific Research (No. FA9550-09-1-0426), the Asian Office of Aerospace R&D (No. FA2386-11-1-4072), and the Office of Naval Research (No. N00014-11-1-0300). A.K.-Y.J. thanks the Boeing Foundation for support.

■ REFERENCES

(1) Yang, T.; Wang, M.; Duan, C.; Hu, X.; Huang, L.; Peng, J.; Huang, F.; Gong, X. *Energy Environ. Sci.* **2012**, *5* (8), 8208.
(2) Chen, H.-C.; Chen, Y.-H.; Liu, C.-C.; Chien, Y.-C.; Chou, S.-W.; Chou, P.-T. *Chem. Mater.* **2012**, *24* (24), 4766.
(3) Zhou, H.; Yang, L.; You, W. *Macromolecules* **2012**, *45* (2), 607.
(4) He, Z.; Zhong, C.; Su, S.; Xu, M.; Wu, H.; Cao, Y. *Nat. Photonics* **2012**, *6* (9), 591.
(5) Fringuelli, F.; Marino, G.; Taticchi, A.; Grandolini, G. *J. Chem. Soc., Perkin Trans. 2* **1974**, No. 4, 332.
(6) Shiroudi, A.; Zahedi, E. *Chin. J. Chem.* **2011**, *29* (11), 2249.
(7) Patra, A.; Bendikov, M. *J. Mater. Chem.* **2010**, *20* (3), 422.
(8) Zade, S. S.; Zamoshchik, N.; Bendikov, M. *Chem.—Eur. J.* **2009**, *15* (34), 8613.
(9) Kang, I.; An, T. K.; Hong, J.-a.; Yun, H.-J.; Kim, R.; Chung, D. S.; Park, C. E.; Kim, Y.-H.; Kwon, S.-K. *Adv. Mater.* **2013**, *25* (4), 524.
(10) Oyaizu, K.; Iwasaki, T.; Tsukahara, Y.; Tsuchida, E. *Macromolecules* **2004**, *37* (4), 1257.
(11) Heeney, M.; Zhang, W.; Crouch, D. J.; Chabinyc, M. L.; Gordeyev, S.; Hamilton, R.; Higgins, S. J.; McCulloch, I.; Skabara, P. J.; Sparrowe, D.; Tierney, S. *Chem. Commun.* **2007**, *0* (47), 5061.
(12) Dou, L.; Chang, W.-H.; Gao, J.; Chen, C.-C.; You, J.; Yang, Y. *Adv. Mater.* **2013**, *25* (6), 825.
(13) Saadeh, H. A.; Lu, L.; He, F.; Bullock, J. E.; Wang, W.; Carsten, B.; Yu, L. *ACS Macro Lett.* **2012**, *1* (3), 361.
(14) Chen, H.-Y.; Yeh, S.-C.; Chen, C.-T.; Chen, C.-T. *J. Mater. Chem.* **2012**, *22* (40), 21549.
(15) Ikai, T.; Azam, A. K. M. F.; Kuzuba, M.; Kuwabara, T.; Maeda, K.; Takahashi, K.; Kanoh, S. *Synth. Met.* **2012**, *162* (17–18), 1707.
(16) Alghamdi, A. A. B.; Watters, D. C.; Yi, H.; Al-Faifi, S.; Almeataq, M. S.; Coles, D.; Kingsley, J.; Lidzey, D. G.; Iraqi, A. *J. Mater. Chem. A* **2013**, *1*, 5165 (DOI: 10.1039/C3TA00122A).
(17) Shahid, M.; Ashraf, R. S.; Huang, Z.; Kronemeijer, A. J.; McCarthy-Ward, T.; McCulloch, I.; Durrant, J. R.; Sirringhaus, H.; Heeney, M. *J. Mater. Chem.* **2012**, *22* (25), 12817.
(18) Mishra, S. P.; Javier, A. E.; Zhang, R.; Liu, J.; Belot, J. A.; Osaka, I.; McCullough, R. D. *J. Mater. Chem.* **2011**, *21* (5), 1551.
(19) Tong, M.; Cho, S.; Rogers, J. T.; Schmidt, K.; Hsu, B. B. Y.; Moses, D.; Coffin, R. C.; Kramer, E. J.; Bazan, G. C.; Heeger, A. J. *Adv. Funct. Mater.* **2010**, *20* (22), 3959.
(20) Coffin, R. C.; Peet, J.; Rogers, J.; Bazan, G. C. *Nat. Chem.* **2009**, *1* (8), 657.

(21) Chang, J.-F.; Clark, J.; Zhao, N.; Sirringhaus, H.; Breiby, D. W.; Andreasen, J. W.; Nielsen, M. M.; Giles, M.; Heeney, M.; McCulloch, I. *Phys. Rev. B: Condens. Matter Mater. Phys.* **2006**, *74* (11), 115318.
(22) Zen, A.; Pflaum, J.; Hirschmann, S.; Zhuang, W.; Jaiser, F.; Asawapirom, U.; Rabe, J. P.; Scherf, U.; Neher, D. *Adv. Funct. Mater.* **2004**, *14* (8), 757.
(23) Kline, R. J.; McGehee, M. D.; Kadnikova, E. N.; Liu, J.; Fréchet, J. M. J. *Adv. Mater.* **2003**, *15* (18), 1519.
(24) Zhao, X.; Tang, H.; Yang, D.; Li, H.; Xu, W.; Yin, L.; Yang, X. *Chin. J. Chem.* **2012**, *30* (9), 2052.
(25) Yuen, J. D.; Kumar, R.; Zakhidov, D.; Seifter, J.; Lim, B.; Heeger, A. J.; Wudl, F. *Adv. Mater.* **2011**, *23* (33), 3780.
(26) Xu, Y.-X.; Chueh, C.-C.; Yip, H.-L.; Ding, F.-Z.; Li, Y.-X.; Li, C.-Z.; Li, X.; Chen, W.-C.; Jen, A. K.-Y. *Adv. Mater.* **2012**, *24* (47), 6356.
(27) Roncali, J. *Macromol. Rapid Commun.* **2007**, *28* (17), 1761.
(28) Hertel, D.; Scherf, U.; Bässler, H. *Adv. Mater.* **1998**, *10* (14), 1119.
(29) Schwarz, C.; Bässler, H.; Bauer, I.; Koenen, J.-M.; Preis, E.; Scherf, U.; Köhler, A. *Adv. Mater.* **2012**, *24* (7), 922.
(30) Chang, H.-H.; Tsai, C.-E.; Lai, Y.-Y.; Chiou, D.-Y.; Hsu, S.-L.; Hsu, C.-S.; Cheng, Y.-J. *Macromolecules* **2012**, *45* (23), 9282.
(31) Chen, Y.-L.; Chang, C.-Y.; Cheng, Y.-J.; Hsu, C.-S. *Chem. Mater.* **2012**, *24* (20), 3964.
(32) Wu, J.-S.; Cheng, Y.-J.; Lin, T.-Y.; Chang, C.-Y.; Shih, P.-I.; Hsu, C.-S. *Adv. Funct. Mater.* **2012**, *22* (8), 1711.
(33) Zhang, Y.; Zou, J.; Yip, H.-L.; Chen, K.-S.; Zeigler, D. F.; Sun, Y.; Jen, A. K.-Y. *Chem. Mater.* **2011**, *23* (9), 2289.
(34) McCulloch, I.; Ashraf, R. S.; Biniek, L.; Bronstein, H.; Combe, C.; Donaghey, J. E.; James, D. I.; Nielsen, C. B.; Schroeder, B. C.; Zhang, W. *Acc. Chem. Res.* **2012**, *45* (5), 714.
(35) Zou, J.; Yip, H.-L.; Zhang, Y.; Gao, Y.; Chien, S.-C.; O'Malley, K.; Chueh, C.-C.; Chen, H.; Jen, A. K.-Y. *Adv. Funct. Mater.* **2012**, *22* (13), 2804.
(36) Chan, S.-H.; Chen, C.-P.; Chao, T.-C.; Ting, C.; Lin, C.-S.; Ko, B.-T. *Macromolecules* **2008**, *41* (15), 5519.
(37) Sun, Y.; Chien, S.-C.; Yip, H.-L.; Chen, K.-S.; Zhang, Y.; Davies, J. A.; Chen, F.-C.; Lin, B.; Jen, A. K.-Y. *J. Mater. Chem.* **2012**, *22* (12), 5587.
(38) Zhang, Y.; Zou, J.; Yip, H.-L.; Chen, K.-S.; Davies, J. A.; Sun, Y.; Jen, A. K. Y. *Macromolecules* **2011**, *44* (12), 4752.
(39) Chen, K.-S.; Zhang, Y.; Yip, H.-L.; Sun, Y.; Davies, J. A.; Ting, C.; Chen, C.-P.; Jen, A. K.-Y. *Org. Electron.* **2011**, *12* (5), 794.
(40) Chen, Y.-C.; Yu, C.-Y.; Fan, Y.-L.; Hung, L.-I.; Chen, C.-P.; Ting, C. *Chem. Commun.* **2010**, *46* (35), 6503.
(41) Zhang, Y.; Chien, S.-C.; Chen, K.-S.; Yip, H.-L.; Sun, Y.; Davies, J. A.; Chen, F.-C.; Jen, A. K.-Y. *Chem. Commun.* **2011**, *47* (39), 11026.
(42) Guo, X.; Zhang, M.; Tan, J.; Zhang, S.; Huo, L.; Hu, W.; Li, Y.; Hou, J. *Adv. Mater.* **2012**, *24* (48), 6536.
(43) Yang, X.; Chueh, C.-C.; Li, C.-Z.; Yip, H.-L.; Yin, P.; Chen, H.; Chen, W.-C.; Jen, A. K.-Y. *Adv. Energy Mater.* **2013**, *3*, 666 (DOI: 10.1002/aenm.201200726).
(44) Zhou, H.; Yang, L.; Stuart, A. C.; Price, S. C.; Liu, S.; You, W. *Angew. Chem., Int. Ed.* **2011**, *50* (13), 2995.
(45) Uy, R. L.; Price, S. C.; You, W. *Macromol. Rapid Commun.* **2012**, *33* (14), 1162.
(46) Bronstein, H.; Ashraf, R. S.; Kim, Y.; White, A. J. P.; Anthopoulos, T.; Song, K.; James, D.; Zhang, W.; McCulloch, I. *Macromol. Rapid Commun.* **2011**, *32* (20), 1664.
(47) Kronemeijer, A. J.; Gili, E.; Shahid, M.; Rivnay, J.; Salleo, A.; Heeney, M.; Sirringhaus, H. *Adv. Mater.* **2012**, *24* (12), 1558.
(48) Wudl, F. *Acc. Chem. Res.* **1984**, *17* (6), 227.
(49) Ha, J. S.; Kim, K. H.; Choi, D. H. *J. Am. Chem. Soc.* **2011**, *133* (27), 10364.
(50) Cocherel, N.; Poriel, C.; Rault-Berthelot, J.; Barrière, F.; Audebrand, N.; Slawin, A. M. Z.; Vignau, L. *Chem.—Eur. J.* **2008**, *14* (36), 11328.
(51) O'Malley, K. M.; Li, C.-Z.; Yip, H.-L.; Jen, A. K.-Y. *Adv. Energy Mater.* **2012**, *2* (1), 82.
(52) Li, C.-Z.; Chueh, C.-C.; Yip, H.-L.; O'Malley, K. M.; Chen, W.-C.; Jen, A. K.-Y. *J. Mater. Chem.* **2012**, *22* (17), 8574.